In-situ GISAXS observation of ion-induced nanoscale pattern formation on crystalline Ge(001) in the reverse epitaxy regime

Denise J. Erb,¹ Peco Myint,^{2,3} Kenneth Evans-Lutterodt,⁴ Karl Ludwig,^{2,5} and Stefan Facsko¹

¹Ion Beam Center, Institute of Ion Beam Physics and Materials Research,
Helmholtz-Zentrum Dresden-Rossendorf, Dresden, Germany

² Division of Materials Science and Engineering, Boston University, Boston, Massachusetts, USA

³X-ray Science Division, Argonne National Laboratory, Lemont, Illinois 60439, USA

⁴National Synchrotron Light Source II, Brookhaven National Lab, Brookhaven, New York, USA

⁵Department of Physics, Boston University, Boston, Massachusetts, USA

(Dated: October 5, 2021)

The ion-induced nanoscale pattern formation on a crystalline Ge(001) surface is observed *in-situ* by means of Grazing Incidence Small Angle X-ray Scattering (GISAXS). Analysis of the GISAXS intensity maps yields the temporal development of geometric parameters characterizing the changing pattern morphology. In comparison with theoretical predictions and with simulations of the patterning process based on a continuum equation we find good agreement for the temporal evolution of the polar facet angle, characteristic length, and surface roughness in the non-linear regime. To achieve this agreement, we included an additional term in the continuum equation which adjusts the pattern anisotropy.

I. INTRODUCTION

Irradiating a solid surface with low-energy ions can lead to various effects on the nanoscale surface topography [1-3], ranging from smoothing [4] to the formation of ripple or dot patterns [5, 6] to the self-assembly of faceted and highly regular morphologies [7]. From the perspective of fundamental science, nanoscale pattern formation under ion-irradiation is considered an example of complex nonequilibrium dynamics; the observable patterns are the result of the interplay of numerous erosive, ballistic, and diffusive mechanisms on the atomic scale. While different aspects of the patterning process still require clarification and remain the subject of ongoing investigations [3, 8–10], researchers from other fields of fundamental science as well as from applied sciences have taken up employing ion-induced pattern formation in bottom-up nanofabrication of functional materials for magnetism [11], plasmonics [12], or sensing [13]. Ion-induced patterning has turned out to occur on a large number of materials and to be widely tunable via external control parameters. Thus, it is a highly versatile technique for many applications where large areas of nanostructured surfaces or thin films are required. Both fundamental and applied research may benefit from in-situ studies revealing the time-dependent development of the patterning process, yielding further insight into the dominant mechanisms and thus enabling to gain precise control of the patterning process.

The surface-sensitive X-ray scattering technique of Grazing Incidence Small Angle X-Ray Scattering (GISAXS) [14] is a well-suited method for such *in-situ* investigations, allowing for contact-less examination of surface morphologies under defined external conditions. Previous

experimental work in this field using GISAXS focused on the formation of ripples or dots with no relation to a possible crystallinity of the material [15–20].

Recently, we reported on real-time in-situ GISAXS experiments [9] on crystalline Ge(001). This material is known to form a checkerboard pattern of faceted pyramidshaped pits and mounds, when irradiated with 1 keV Ar+ ions at normal incidence and at temperatures above the recrystallization temperature. The resulting four-fold symmetry of the Ge surface pattern reflects the diamond lattice symmetry of crystalline Ge. The surface instability is due to the Ehrlich-Schwoebel (ES) barrier for the diffusion of surface vacancies and ad-atoms, which are produced in the collision cascade caused by the ion impact [21]. Owing to its analogy with epitaxial growth, this type of ion-induced patterning is called reverse epitaxy. This recent GISAXS study focused on the regime of reverse epitaxy pattern formation which can be described by linear theory, and compared high temperature patterning with room temperature smoothing to obtain a quantitative estimate of the ES contribution to surface instability under ion irradiation.

Here, we present a real-time *in-situ* GISAXS investigation which extends into the non-linear regime of patterning in crystalline Ge(001). From different characteristic features of the angular distribution of scattered xray intensity we deduce the characteristic length and the polar facet angle to describe the development of the surface morphology with time during ion irradiation. These are compared with the according results from simulations based on a continuum equation of the local surface height to model the morphology development including ballistic and diffusive processes. Experiment and theoretical model are found to be in good agreement, allowing us to relate GISAXS intensity maps in reciprocal space to simulated

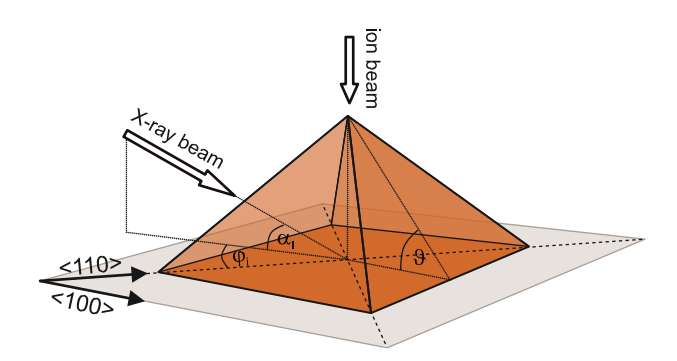


FIG. 1. Sketch of a pyramidal nanostructure expected to form on the crystalline Ge(001) surface due to normal-incidence ion irradiation as indicated by the vertical arrow. Black arrows show the crystal orientations of the Ge(001) surface. The white arrow indicates the direction of the incident X-ray beam with respect to the orientation of the nanostructure for ϕ_i = 45°. ϑ denotes the polar facet angle of the nanostructure, which is identical for all four pyramid side walls.

surface topographies in real-space. While the linear regime at very early times could not be accessed given the available time resolution in the experiment, we observed the temporal evolution of facet angles and characteristic length in the non-linear regime. In particular, we find that the facet angle kinetics can be described by the Austin-Rickett equation for diffusion-controlled transformation processes. The temporal evolutions of characteristic length and roughness conform to power laws. Their exponents agree with scaling laws for conserved continuum equations with four-fold symmetry.

II. EXPERIMENTAL PROCEDURES AND RESULTS

The in-situ GISAXS experiment was conducted at the Integrated In-Situ and Resonant Hard X-ray Studies (ISR) beamline of the NSLS-II synchrotron X-ray source at Brookhaven National Lab, employing a custom-made UHV chamber with a base pressure of $p_0 = 10^{-6}$ mbar. Polished Ge(001) samples were wiped with ethanol and then mounted in the chamber such that either the h100i or the h110i direction was parallel to the azimuthal direction of the incident X-ray beam ($\phi_i = 0^\circ$ or $\phi_i = 45^\circ$), with the polar X-ray incidence angle being $\alpha_i = 0.43^\circ$. We used X-rays with an energy of $E_X = 11.51$ keV, corresponding to a wavelength $\lambda_X = 0.1077$ nm, and a Dectris Eiger 1M area detector with 0.075 mm pixel size at a distance of D = 2490 mm from the sample position. Both samples were irradiated with a broad beam of Ar+ ions with a kinetic energy of $E_{kin} = 1$ keV and a flux of $\varphi = 1 \times 10^{15}$ cm⁻²s⁻¹ from a Kaufman-type ion source (manufacturer: Veeco, collimation grid diameter: 3 cm) at normal incidence. After an initial irradiation at room temperature for removing the native oxide, the samples were heated to T = 260 °C, with the temperature being measured by a thermocouple attached to the sample support plate. During irradiation at 260 °C, GISAXS intensity maps were recorded every 10 s with 10 s exposure time for 3600 s. After irradiation, additional GISAXS intensity maps were recorded with each sample rotated by 45°. The final surface topography was imaged *ex-situ* by atomic force microscopy (AFM), using a Bruker MultiMode8 setup in tapping mode under ambient conditions. The software packages FIJI ImageJ [22] and FitGISAXS [23] were used for processing and plotting GISAXS data. Peak positions and widths were extracted from horizontal sections through the GISAXS patterns by means of an Octave script. AFM data were processed and analyzed using the software package gwyddion [24].

A. In-situ GISAXS

Figure 2 displays sequences of GISAXS intensity maps for two Ge(001) samples A (top row) and B (bottom row) during irradiation with Ar+ ions, with the x-ray incidence direction parallel to h100i for subfigures (ad) and parallel to h110i for (f-i), respectively. The labels state the time elapsed after starting the ion irradiation. Maps (e) and (j) were recorded after ion irradiation, with the respective sample rotated azimuthally by 45°. The development of three characteristic features can be observed in the intensity maps: Firstly, intensity maxima in a horizontal section at $\alpha_f = 0.2^{\circ}$ form and move in toward the vertical specular scattering rod at $2\theta_f = 0^\circ$. This corresponds to the formation of a surface pattern with a well-defined lateral characteristic length $L = \lambda_X/(\sin 2\theta_f \cos \alpha_f) \approx \lambda_X/\sin 2\theta_f [14]$ and to the increase of this characteristic length to L_A = (130 ± 5) nm and $L_B = (118\pm5)$ nm, respectively, after 3600 s of ion irradiation. Secondly, tilted scattering rods form and increase their tilt angle with respect to the orientation of the vertical specular scattering rod. These tilted scattering rods are identified as crystal truncation rods (CTRs) originating from parts of the surface which are tilted with respect to the initial sample surface, i.e. the side walls of the faceted pyramidal surface structures [25]. The tilt angle β of the CTRs relates to the polar inclination angle ϑ (as measured from the initial surface plane) of the surface areas they originate from as $\tan \beta = \tan \theta \cos \phi_i$ [26]. Thus, changes in the CTR angle directly correspond to changes in the polar orientation of surface facets. After 3600 s of ion irradiation, the GISAXS data show an average polar facet angle of $\theta = (11 \pm 1)^{\circ}$. Thirdly, the intensity of the tilted truncation rods increases at the expense of the specularly scattered intensity at $2\theta_f = 0^\circ$. This evidences that an increasing fraction of the surface area becomes tilted until the sample surface is finally fully patterned with faceted pyramidal structures (see AFM topography measurements in Fig. 3). We will discuss how the characteristic length L and the polar facet angle ϑ develop with irradiation duration in comparison with simulation results.

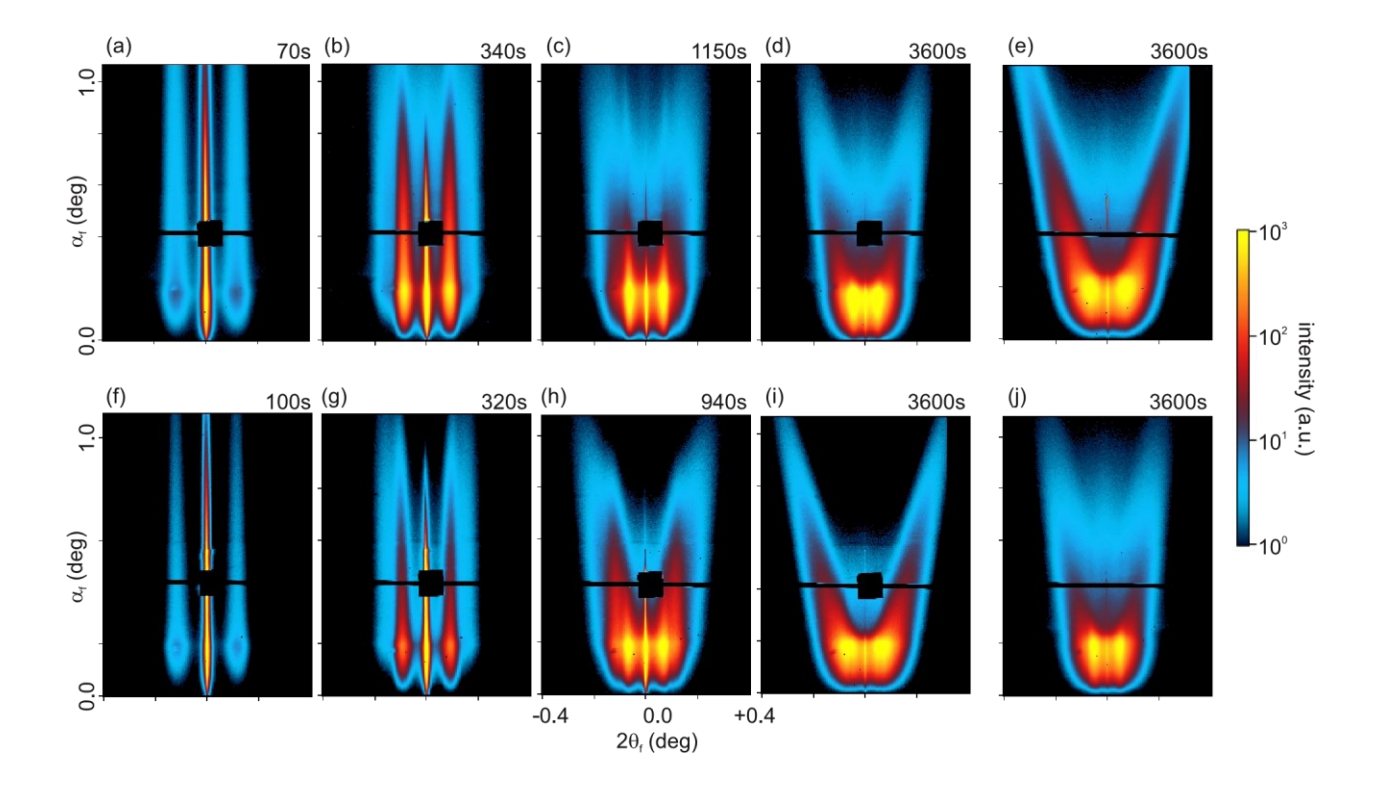


FIG. 2. GISAXS intensity maps for two samples recorded at different azimuthal orientations with respect to the direction of the incident X-ray beam. Sample A (top row): ϕ_i = 45° during irradiation (a-d) and ϕ_i = 0° after ion irradiation (e). Sample B (bottom row): ϕ_i = 0° during irradiation (f-i) and ϕ_i = 45° after irradiation (j). The intense specular reflection is blocked by a square-shaped beamstop to avoid damage to the detector. After irradiation and pattern formation on the surface the specular reflection had become so weak that the beamstop could be removed for the final intensity maps.

B. Ex-situ AFM

Figure 3 shows the final topography of the Ge surface after ion irradiation. As observed before [21], the surface exhibits a faceted pattern of alternating pits and mounds with pyramidal shape. The patterned surfaces of samples A and B have a roughness of 4.4 nm and 3.8 nm, respectively. The small difference in roughness can be attributed to several factors, e.g. the choice of the AFM measurement region or small differences in sample temperature, ion flux, or initial surface conditions. In agreement with the results from the GISAXS experiments, the characteristic lengths obtained from power spectral density functions of the AFM topography data are L_A = (120±10) nm and $L_B = (118\pm10)$ nm, respectively. The pyramid bases align with the h100i and h010i directions, and the pyramid side walls exhibit a polar inclination of ϑ = (11 ± 1) ° as measured from the initial surface normal, in very good agreement with the in-situ GISAXS data. These facets can be identified with the (105) planes of the Ge crystal [7].

III. THEORETICAL DESCRIPTION AND SIMULATION RESULTS

The temporal evolution of the local surface height h(x,y,t) of the crystalline Ge(001) surface under normalincidence ion irradiation can be described by the following continuum equation [21]

$$\partial_t h = -\mathbf{v}_0 + \nu \nabla^2 h + \lambda (\nabla h)^2 - \nabla \cdot \mathbf{j}_{\text{diff}} \tag{1}$$

Eq. 1 includes sputter erosion and mass redistribution

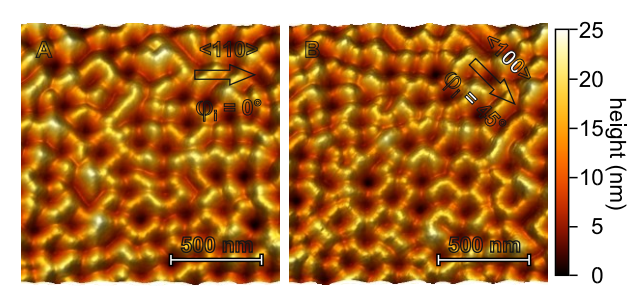


FIG. 3. AFM surface topography measurement of samples A and B after 3600 s of ion irradiation. The arrows indicate the azimuthal incidence direction of the X-ray beam during ion irradiation.

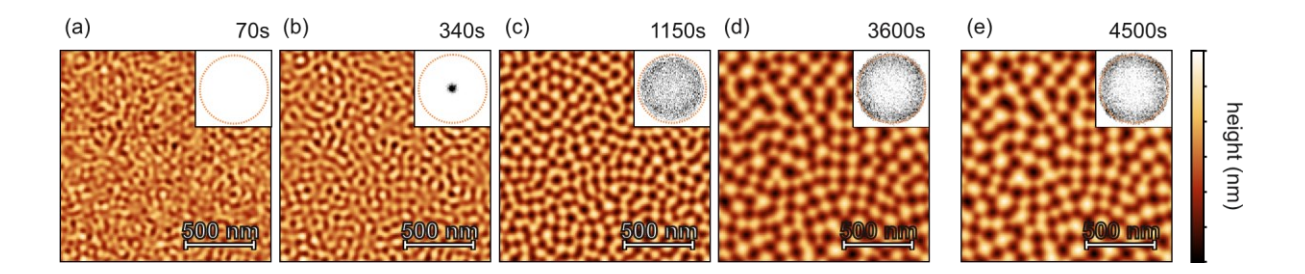


FIG. 4. Simulated development of the Ge(001) surface topography under ion irradiation with increasing irradiation duration from left to right. (a-d) correspond to the time steps in Fig. 2, while (e) depicts the topography after 4500 seconds. The height scale indicated by the false color ruler ranges from 0 to (a) 0.125 nm (b) 2 nm (c) 11.5 nm (d,e) 20 nm. The insets show two-dimensional angle distributions of the topographies, with the dotted ring indicating the final polar angle of θ = 11.5°.

due to ballistic and diffusive processes as well as a noise term η : v_0 is the constant rate of erosion for a planar surface. $v\nabla^2 h$ denotes the curvature-dependent sputter rate and ballistic mass redistribution according to the Bradley-Harper theory [27] and the Carter-Vishnyakov effect [28], respectively. $\lambda(\nabla h)^2$ accounts for the tiltdependent sputtering [29, 30]. Finally, j_{diff} describes the diffusive mass currents on a (001)surface with square symmetry as [31, 32]

$$\begin{aligned} \textit{j}_{\text{diff}} &= \textit{j}_{\text{CKPZ}} + \textit{j}_{\text{HM}} + \textit{j}_{\text{ES}} \\ &= \sigma \nabla \left(\nabla h \right)^2 + \kappa \nabla (\nabla^2 h) + \\ &+ \epsilon \left[\frac{\partial_x h - \delta \left(\partial_x h \right)^3 - \gamma \delta \left(\partial_y h \right)^3}{\partial_y h - \delta \left(\partial_y h \right)^3 - \gamma \delta \left(\partial_x h \right)^3} \right] \end{aligned} \tag{2}$$

The diffusive mass currents can be isotropic or anisotropic in nature: The conserved Kadar-Parisi-Zhang term **j**_{CKPZ} describes a non-linear mass current which leads to up-down symmetry breaking of the surface pattern [33]. *i*_{HM} is an isotropic current likened to HerringMullins diffusion [34], resulting in smoothing of the surface. ies accounts for anisotropic diffusion due to the Ehrlich-Schwoebel and kink barriers in x- and y-direction, i.e. biased diffusion across terrace steps and around kinks on a crystalline surface [35–38]. This term results in effective uphill mass currents and the formation of facets with inclination θ = arctan(sqrt(1/ δ)) for which this mass current becomes zero [21, 31]. The parameter γ accounts for the degree of the anisotropy of the surface currents. For $\gamma = 1$ the resulting patterns are fully anisotropic, whereas for $\gamma = 0$ the surface currents are isotropic, resulting in an isotropic pits and mounds pattern. Microscopically, the degree of anisotropy can be linked to the height of the kink barrier. The height evolution described by this continuum equation is dominated by the linear terms early in the process for small t (the linear regime), while the nonlinear terms dominate later in the process for large t (the non-linear regime).

We simulated how the surface topography of Ge(001) develops under normal-incidence ion irradiation by numerical integration [39] of Eq. 1 with $v_0 = 0$ (i.e. disregarding a homogeneous erosion of the entire surface at constant rate), v = 0 and $\lambda = 0$ (i.e. neglecting any curvature dependent sputtering and ballistic mass redistribution effects), $\sigma = 0$ (i.e. assuming a surface morphology with up-down symmetry), $\kappa = 4, \epsilon = 0.5, \delta_{=}$ 25, and γ = 0.9. Thus, the simulation considers the isotropic and anisotropic diffusion on the surface under ion irradiation as clearly dominant, while erosive and ballistic effects are regarded as negligible. This approach has been shown to describe the pattern formation in reverse epitaxy regime at normal incidence ion irradiation quite well [10, 21]. In order to reproduce the experimentally observed development of the characteristic length L and the polar facet angle ϑ , the anisotropy degree γ has to be close to 1, indicating a small kink barrier. The temporal and lateral dimensions are scalable, i.e. they have arbitrary units – we scaled them as follows to match the experiment: t_{exp} = 12.29 s × t_{sim} and x_{exp} = 3.02 nm × x_{sim} . The simulation starts from a planar surface an initial uncorrelated rootmean-square roughness of 0.06 nm.

IV. DISCUSSION

Fig. 4 shows individual frames from the simulation, illustrating the topography development with time. The time steps for Fig. 4(a-d) correspond to those in the sequence of GISAXS intensity maps in Fig. 2(a-d),(f-i). In addition, subfigure (e) shows the simulated surface topography in a further advanced state after 4500 s. The insets display two-dimensional angular distributions. We find very good qualitative agreement with the *ex-situ* AFM data regarding the shape and orientation of the pyramidal surface structures. In agreement with the *in-situ* GISAXS data we observe coarsening, i.e. an increase of the characteristic length with time, as well as a progressive expression of faceted structures with increasingly well-defined polar angles and thereby faceting of the entire surface area.

For a quantitative comparison between experiment and simulation, we extracted the polar facet angles ϑ and characteristic length L from the GISAXS data of sample A and from the sequence of simulated surface patterns,

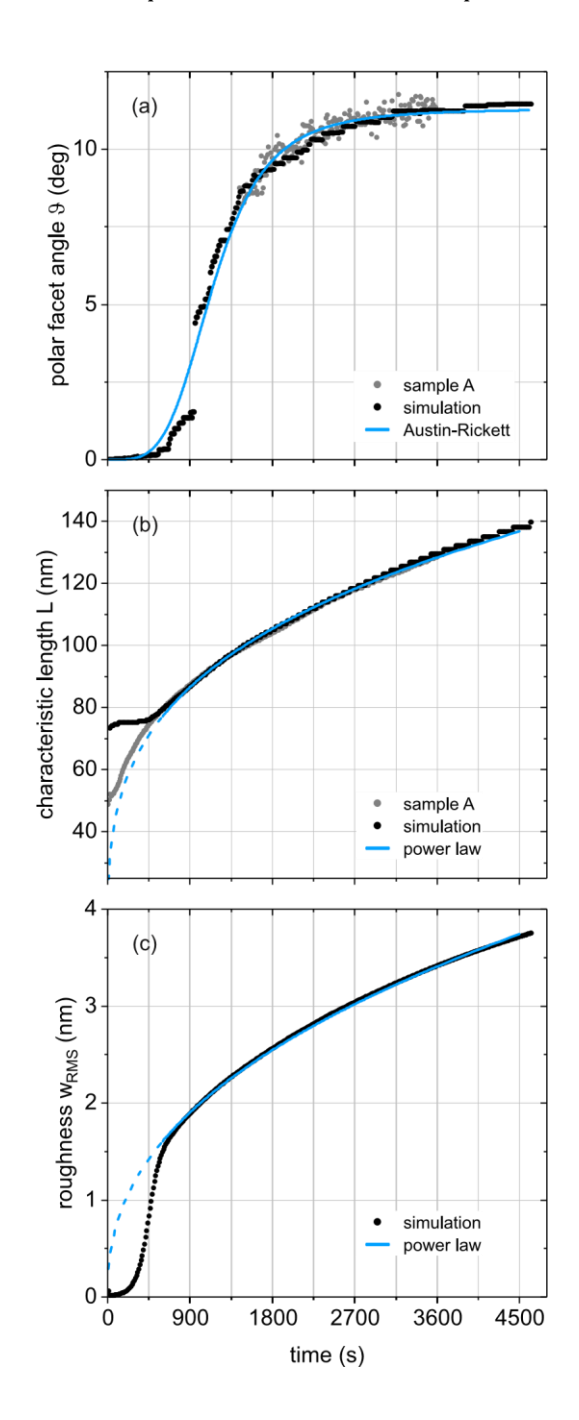


FIG. 5. Kinetics of (a) polar facet angle ϑ , (b) characteristic length L, and (c) root-mean-square roughness w_{RMS} obtained from experiment and simulation. Solid lines show fits to the data; see main text for details.

see Fig. 5(a). The GISAXS data allow for measuring ϑ starting from an irradiation duration of approx. t = 1400 s, when the tilted scattering rods are sufficiently well separated from the vertical ones. For the simulated data, ϑ was determined starting from t = 0 by locating the maxima in the polar angle histogram [40]. However, for t < 900 s, when the maxima in the histogram are not well separated, this approach underestimates the value of ϑ . For later times, the polar facet angle found in the experiments is well reproduced in the simulation, and the temporal evolution of both can be fitted well by an Austin-Rickett equation

$$\vartheta(t) = \vartheta_0 \left(1 - \frac{1}{(kt)^n + 1} \right) \tag{3}$$

with $\theta_0 = 11.30$, $k = 8.63 \times 10^{-4}$, n = 4. The Austin-

Rickett equation is commonly used to describe diffusion-controlled structural transformations proceeding via nucleation and growth [41]. It thus appears appropriate and feasible here for modeling the kinetics of the polar facet angle. Since it requires the exponent n to be an integer multiple of 0.5, n was fixed while ϑ_0 and k were fitted.

The temporal development of the characteristic length [40] is plotted in Fig. 5(b) in comparison to a power law, given by

$$L(t) = at^{1/z} \tag{4}$$

with a = 12.54 and a coarsening exponent of 1/z = 0.28. The continuum equation predicts a constant characteristic length in the linear regime and coarsening of pattern periodicity to set in later in the non-linear regime [27]. This behavior is clearly observed in the development of the simulated characteristic length, with the transition from the linear to the non-linear regime occurring around t = 600 s. For t > 900 s the power law fits both simulated and experimental data very well. The coarsening exponent agrees quite well with the expectation of 1/z = 0.25 from theory and supports and the assumption of a dominant Herring-Mullins surface relaxation term [32] and a pronounced Ehrlich-Schwoebel barrier [36]. It differs from earlier comparable ion irradiation experiments on Ge(001), however, where the surface dynamics were studied using ex-situ AFM and simulations with a smaller grid size [21]. In-situ GISAXS is expected to yield a more reliable measure of the development of the characteristic length with time than ex-situ AFM due to the larger surface area which is probed by GISAXS (µm² for AFM vs. cm² for GISAXS) and due to the improved control of ion fluence in a continuous in-situ experiment. The experimental data show coarsening in approximate agreement with Eq. 4 even for very early times. Therefore, the linear regime appears to be shortened or compressed in the experiment due to a higher initial surface roughness than in the simulation. Indeed, the GISAXS intensity maps show off-specular scattering rods from the first frame on, i.e. after an irradiation duration of 10 s and a fluence of 1×10^{16} cm $^{-2}$. GISAXS data with significantly higher time resolution would have been necessary to identify the linear regime in the experiment.

Fig. 5(c) compares the kinetics of the root-mean-square roughness w_{RMS} obtained from the simulation with a power law fit:

$$w_{RMS}(t) = bt^{\beta} \tag{5}$$

with b=0.11 and $\beta=0.42$. The growth exponent is in fair agreement with the theoretical prediction of $\beta=0.5$ [32]. Again, the simulation deviates markedly from a power-law behavior for early times of t<600 s, i.e. in the linear regime, where an exponential increase is predicted. In the non-linear regime the surface roughening then slows down [27]. The roughness of approximately 3.5 nm obtained from the simulation after 3600 s agrees well with the corresponding experimental results.

V. CONCLUSIONS

In this contribution, we have compared *in-situ* GISAXS data of a crystalline surface under normalincidence lowenergy ion irradiation with simulations based on numerical integration of a continuum equation. We observe how the surface morphology evolves by tracking the changes in the polar facet angle, the characteristic length, and the surface roughness with time. Good agreement of the simulation with both experiment and theory was only achieved, when including in the

continuum equation an additional term for regulating the pattern anisotropy. We then find that a continuum equation considering only diffusive effects reproduces the experimentally observed temporal evolution well in the non-linear regime of ion irradiation: The characteristic length increases with time (i.e., ion fluence) according to a power law, with coarsening exponent 1/z = 0.28. An Austin-Rickett equation with exponent n = 4 describes the development of the polar facet angle, corroborating our assumption of a diffusion-controlled process. The simulated roughness conforms to a power law dependence with a growth exponent of $\beta = 0.42$. Thus, this extended continuum equation also is in agreement with established theoretical predictions on pattern formation.

ACKNOWLEDGMENTS

We thank David Babonneau for helpful discussions. The experimental part of this work was carried out using beamline ISR (4-ID) of the National Synchrotron Light Source II, a U.S. Department of Energy (DOE) Office of Science User Facility operated for the DOE Office of Science by Brookhaven National Laboratory under Contract No. DE-SC0012704, and facilities of the Ion Beam Center at Helmholtz-Zentrum Dresden-Rossendorf, a member of the Helmholtz Association. The work at Boston University was partly supported by the National Science Foundation under Grant No. DMR-2117509.

^[1] U. Valbusa, C. Boragno, and F. Buatier de Mongeot, Nanostructuring surfaces by ion sputtering, J. Phys.: Condens. Matter **14**, 8153 (2002).

^[2] W. L. Chan and E. Chason, Making waves: Kinetic processes controlling surface evolution during low energy ion sputtering, J. Appl. Phys. **101**, 121301 (2007).

^[3] R. Cuerno and J.-S. Kim, A perspective on nanoscale pattern formation at surfaces by ion-beam irradiation, J. Appl. Phys. **128**, 180902 (2020).

^[4] M. Moseler, P. Gumbsch, C. Casiraghi, A. C. Ferrari, and J. Robertson, The Ultrasmoothness of Diamond-like Carbon Surfaces, Science **309**, 1545 (2005).

^[5] S. Rusponi, G. Costantini, C. Boragno, and U. Valbusa, Ripple Wave Vector Rotation in Anisotropic Crystal Sputtering, Phys. Rev. Lett. **81**, 2735 (1998).

^[6] S. Facsko, T. Dekorsy, C. Koerdt, C. Trappe, H. Kurz, A. Vogt, and H. L. Hartnagel, Formation of Ordered Nanoscale Semiconductor Dots by Ion Sputtering, Science 285, 1551 (1999).

^[7] X. Ou, K.-H. Heinig, R. Hu bner, J. Grenzer, X. Wang, M. Helm, J. Fassbender, and S. Facsko, Faceted nanostructure arrays with extreme regularity by self-assembly of vacancies, Nanoscale 7, 18928 (2015).

^[8] S. A. Norris and M. J. Aziz, Ion-induced nanopatterning of silicon: Towards a predictive model, Appl. Phys. Rev. 6, 011311 (2019).

^[9] P. Myint, D. Erb, X. Zhang, L. Wiegart, Y. Zhang, A. Fluerasu, R. L. Headrick, S. Facsko, and K. F. Ludwig, Measurement of Ehrlich-Schwoebel barrier contribution to the selforganized formation of ordered surface patterns on Ge(001), Phys. Rev. B 102, 201404(R) (2020).

^[10] D. Erb, R. de Schultz, A. Ilinov, K. Nordlund, R. M. Bradley, and S. Facsko, Nanopatterning of the (001) surface of crystalline Ge by ion irradiation at off-normal incidence: Experiment and simulation, Phys. Rev. B 102, 165422 (2020).

^[11] M. O. Liedke, M. Koʻrner, K. Lenz, M. Fritzsche, M. Ranjan, A. Keller, E. Ciʻzmar, S. A. Zvyagin, S. Facsko, K. Potzger, J. Lindner, and J. Fassbender, Crossover in the surface anisotropy contribution of ferromagnetic films on rippled Si surfaces, Phys. Rev. B **87**, 024424 (2013).

^[12] A. Toma, D. Chiappe, D. Massabo`, C. Boragno, and F. Buatier de Mongeot, Self-organized metal nanowire arrays with tunable optical anisotropy, Appl. Phys. Lett. **93**, 163104 (2008).

^[13] D. Gkogkou, B. Schreiber, T. Shaykhutdinov, H. K. Ly, U. Kuhlmann, U. Gernert, S. Facsko, P. Hildebrandt, N. Esser, K.

- Hinrichs, I. M. Weidinger, and T. W. H. Oates, Polarizationand WavelengthDependent Surface-Enhanced Raman Spectroscopy Using Optically Anisotropic Rippled Substrates for Sensing, ACS Sensors 1, 318 (2016).
- [14] G. Renaud, R. Lazzari, and F. Leroy, Probing surface and interface morphology with Grazing Incidence Small Angle X-Ray Scattering, Surf. Sci. Rep. 64, 255 (2009).
- [15] F. Ludwig, Jr., C. R. Eddy, Jr., O. Malis, and R. L. Headrick, Si(100) surface morphology evolution during normalincidence sputtering with 100–500 eV Ar+ions, Appl. Phys. Lett. 81, 2770 (2002).
- [16] H. Zhou, Y. Wan, L. Zhau, R. L. Headrick, A. S. Ozcan,"
 Y. Wang, G. Ozaydin, K. F. Ludwig, and D. P. Siddons,"
 Wavelength tunability of ion-bombardment-induced ripples on sapphire, Phys. Rev. B **75**, 155416 (2007).
- [17] A. Keller, A. Biermanns, G. Carbone, J. Grenzer, S. Facsko, O. Plantevin, R. Gago, and T. H. Metzger, Transition from smoothing to roughening of ion-eroded GaSb surfaces, Appl. Phys. Lett. **94**, 193103 (2009).
- [18] O. Bikondoa, D. Carbone, V. Charmard, and T. H. Metzger, Ageing dynamics of ion bombardment induced selforganization processes, Sci. Rep. **3**, 1850 (2013).
- [19] S. A. Norris, J. C. Perkinson, M. Mokhtarzadeh, E. Anzenberg, M. J. Aziz, and K. F. Ludwig, Distinguishing physical mechanisms using GISAXS experiments and linear theory: the importance of high wave numbers, Sci. Rep. 7 (2016).
- [20] D. Babonneau, E. Vandenhecke, and S. Camelio, Formation of nanoripples on amorphous alumina thin films during low-energy ion-beam sputtering: Experiments and simulations, Phys. Rev. B **95**, 085412 (2017).
- [21] X. Ou, A. Keller, M. Helm, J. Fassbender, and S. Facsko, Reverse Epitaxy of Ge: Ordered and Faceted Surface Patterns, Phys. Rev. Lett. **111**, 016101 (2013).
- [22] J. Schindelin, I. Arganda-Carreras, E. Frise, V. Kanig, M. Longair, T. Pietzsch, S. Preibisch, C. Rueden, S. Saalfeld, B. Schmid, J.-Y. Tinevez, D. J. White, V. Hartenstein, K. Eliceiri, P. Tomancak, and A. Cardona, Fiji: an open-source platform for biological image analysis, Nature Methods 9, 676 (2012).
- [23] D. Babonneau, FitGISAXS: software package for modelling and analysis of GISAXS data using IGOR Pro, J. Appl. Cryst. 43, 929 (2010).
- [24] D. Ne´cas and P. Klapetek, Gwyddion: an open-source software for SPM data analysis, Central European Journal of Physics 10, 181 (2012).
- [25] C. Revenant, F. Leroy, G. Renaud, R. Lazzari, A. L'etoublon, and T. Madey, Structural and morphological evolution of Co on faceted Pt/W(111) surface upon thermal annealing, Surf. Sci. **601**, 3431 (2007).
- [26] T. David, D. Buttard, T. Schu'lli, F. Dallhuin, and P. Gentile, Structural investigation of silicon nanowires using GIXD and GISAXS: Evidence of complex sawtooth faceting, Surface Science **602**, 2675 (2008).
- [27] R. M. Bradley and J. M. E. Harper, Theory of ripple topography induced by ion bombardment, J. Vac. Sci. Technol. A 6, 2390 (1988).
- [28] G. Carter and V. Vishnyakov, Roughening and ripple instabilities on ion-bombarded Si, Phys. Rev. B **54**, 17647 (1996).

- [29] R. Cuerno and A. L. Baraba´si, Dynamic scaling of ionsputtered surfaces, Phys. Rev. Lett. **74**, 4746 (1995).
- [30] B. Davidovitch, M. J. Aziz, and M. P. Brenner, On the stabilization of ion sputtered surfaces, Phys. Rev. B 76, 205420 (2007).
- [31] M. Siegert, Coarsening Dynamics of Crystalline Thin Films, Phys. Rev. Lett. **81**, 5481 (1998).
- [32] L. Golubovi'c, A. Levandovsky, and D. Moldovan, Interface Dynamics and Far-From-Equilibrium Phase Transitions in Multilayer Epitaxial Growth and Erosion on Crystal Surfaces: Continuum Theory Insights, E. Asia. J. Appl. Math. 1, 297 (2011).
- [33] M. Kardar, G. Parisi, and Y.-C. Zhang, Dynamic Scaling of Growing Interfaces, Phys. Rev. Lett. **56**, 889 (1986).
- [34] W. W. Mullins, Flattening of a Nearly Plane Solid Surface due to Capillarity, J. Appl. Phys. **30**, 77 (1959).
- [35] J. Villain, Continuum models of crystal growth from atomic beams with and without desorption, J. Phys I 1, 19 (1991).
- [36] J. G. Amar and F. Family, Step-Adatom Attraction as a New Mechanism for Instability in Epitaxial Growth, Phys. Rev. Lett. 77, 4584 (1996).
- [37] Z. Zhang and M. G. Lagally, Atomistic Processes in the Early Stages of Thin-Film Growth, Science 276, 377 (1997).
- [38] O. Pierre-Louis, M. R. D'Orsogna, and T. L. Einstein, Edge Diffusion during Growth: The Kink EhrlichSchwoebel Effect and Resulting Instabilities, Phys. Rev. Lett. 82, 3661 (1999).
- [39] A. Keller, S. Facsko, and R. Cuerno, Numerical Integrator for Continuum Equations of Surface Growth and Erosion, in *Computational Nanotechnology: Modeling and Applications with MATLAB*, edited by S. M. Musa (CRC Press, 2012) Chap. 5, pp. 189–215.
- [40] See supplemental material for details on the determination of the characteristic length from the GISAXS data and on the determination of the polar facet angle from the simulated topographies.
- [41] M. Starink, Kinetic equations for diffusion-controlled precipitation reactions, J. Mater. Sci. **32**, 4061 (1997).